Acta Crystallographica Section D
Biological Crystallography
ISSN 1399-0047

Efficient calculation of diffracted intensities in the case of nonstationary scattering by biological macromolecules under XFEL pulses

Vladimir Y. Lunin,[a]* Alexei N. Grum-Grzhimailo,[b] Elena V. Gryzlova,[b] Dmitry O. Sinitsyn,[c] Tatiana E. Petrova,[a] Natalia L. Lunina,[a] Nikolai K. Balabaev,[a] Ksenia B. Tereshkina,[c] Alexei S. Stepanov[c] and Yurii F. Krupyanskii[c]

[a]Institute of Mathematical Problems of Biology, Russian Academy of Sciences, Pushchino 142290, Moscow Region, Russian Federation, [b]Skobeltsyn Institute of Nuclear Physics, Lomonosov Moscow State University, Moscow 119991, Russian Federation, and [c]Semenov Institute of Chemical Physics, Russian Academy of Sciences, 4 Kosygina Street, Moscow 119991, Russian Federation

Correspondence e-mail: lunin@impb.psn.ru

Received 20 May 2014
Accepted 20 November 2014

The calculation of diffracted intensities from an atomic model is a routine step in the course of structure solution, and its efficiency may be crucial for the feasibility of the study. An intense X-ray free-electron laser (XFEL) pulse can change the electron configurations of atoms during its action. This results in time-dependence of the diffracted intensities and complicates their calculation. An algorithm is suggested that enables this calculation with a computational cost comparable to that for the time-independent case. The intensity is calculated as a sum of the 'effective' intensity and a finite series of 'correcting' intensities. These intensities are calculated in the conventional way but with modified atomic scattering factors that are specially derived for a particular XFEL experiment. The total number of members of the series does not exceed the number of chemically different elements present in the object under study. This number is small for biological molecules; in addition, the correcting terms are negligible within the parameter range and accuracy acceptable in biological crystallography. The time-dependent atomic scattering factors were estimated for different pulse fluence levels by solving the system of rate equations. The simulation showed that the changes in a diffraction pattern caused by the time-dependence of scattering factors are negligible if the pulse fluence does not exceed the limit that is currently achieved in experiments with biological macromolecular crystals (10^4 photons Å^{-2} per pulse) but become significant with an increase in the fluence to 10^6 or 10^8 photons Å^{-2} per pulse.

1. Introduction

In the last decade, X-ray free-electron lasers (XFELs), which are new sources of ultrashort (down to a few femtoseconds) and ultra-intense X-ray pulses, have been developed. These devices allow one to collect series of single diffraction images from nanometre-sized to micrometre-sized crystals of macromolecules and noncrystalline biological specimens. This has opened up new possibilities for determining the structures of biological species which are difficult to crystallize (*e.g.* membrane proteins). These methodological and technical achievements have led to significant progress in the field of XFEL structure determination. Complete data sets from macromolecular crystals of already known structure have been collected, and the quality of the models and the electron-density maps was comparable with those obtained at synchrotrons (Chapman *et al.*, 2011; Lomb *et al.*, 2011; Johansson *et al.*, 2012; Boutet *et al.*, 2012; Kern *et al.*, 2012). A clear advantage of XFELs over synchrotrons for data collection has been demonstrated for structures that are sensitive to radiation damage (Johansson *et al.*, 2013; Kern *et al.*, 2013). Recently, a protein structure containing a large unknown part

was first solved using XFEL data (Redecke *et al.*, 2013). Very recently, single-wavelength anomalous scattering measurements have been performed using an XFEL (Barends *et al.*, 2013, 2014), and the possibility of determining a protein structure *de novo* has been shown (Barends *et al.*, 2014).

At the same time, numerous theoretical and numerical studies have been concerned with the calculation of diffraction intensities and, in particular, the problem of how strongly a diffraction pattern is affected by radiation damage at such high photon fluences (Quiney & Nugent, 2011; Lorenz *et al.*, 2012; Curwood *et al.*, 2013). The dose that a sample receives during a single pulse at an XFEL can exceed the maximal tolerable dose for a crystal during a whole data-collection run at a modern synchrotron (Henderson, 1995; Chapman *et al.*, 2011; Johansson *et al.*, 2013). The possibility of using an ultrashort pulse length at XFELs allowed the postulation of the so-called 'diffraction-before-destruction' concept, according to which an interpretable diffraction image can be obtained before the sample is destroyed (Neutze *et al.*, 2000; Barty *et al.*, 2012). Electron emission both in atomic photoionization and the Auger process takes place on a time scale of less than 10 fs (Krause & Oliver, 1979; Neutze *et al.*, 2000), whereas the consequent processes of overall damage to the sample (thermalization, breakage of covalent bonds and Coulomb explosion) occur on a much longer time scale (Hau-Riege *et al.*, 2004; Bergh *et al.*, 2008). Thus, our study was performed on the assumption that radiation-induced changes of atomic configurations affect the diffraction intensity, while radiation-induced atomic movements have not yet occurred during the pulse.

In the stationary case, the intensities of diffracted waves are calculated by conventional formulae of the kinematic theory of diffraction,

$$I(\mathbf{s}) = C|\mathbf{F}(\mathbf{s})|^2, \tag{1}$$

$$\mathbf{F}(\mathbf{s}) = \sum_{j=1}^{N_{\rm atoms}} f_j(s)\exp(-B_j s^2/4)\exp[-2\pi i(\mathbf{s},\mathbf{r}_j)]. \tag{2}$$

Here, $\mathbf{s} = (\boldsymbol{\sigma} - \boldsymbol{\sigma}_0)/\lambda$ is the scattering vector and $s = |\mathbf{s}| = 2\sin\theta/\lambda$, where $\boldsymbol{\sigma}_0$, $\boldsymbol{\sigma}$, 2θ and λ are the directions of the incident and diffracted beams, the scattering angle and the beam wavelength (in Å), respectively, $I(\mathbf{s})$ and $\mathbf{F}(\mathbf{s})$ are the intensity and the complex structure factor of a diffracted wave, respectively, $\{\mathbf{r}_j, B_j\}$, $j = 1, \ldots, N_{\rm atoms}$ are the coordinates of the atoms and the atomic displacement parameters (ADPs), and $\{f_j(s)\}$, $j = 1, \ldots, N_{\rm atoms}$ are the atomic scattering factors. The scaling factor C in (1) is an adjustable parameter in the crystallographic refinement and includes, among other things, the duration of X-ray irradiation. We omit this factor in the formulae below, supposing that it is present implicitly. For simplicity, we write the formulae for the case of isotropic ADPs, although they can be extended to the cases of anisotropic ADPs and partial occupancies.

The atomic scattering factor $f_j(s)$ is related to the electron-density distribution in the atom $\rho_j(r)$ by the Fourier sine transform. For an intense X-ray pulse fluence, the number of scattering electrons can change significantly during the pulse so that the electron-density distribution and the scattering factors become time-dependent. The diffraction intensity accumulated during the pulse is in this case

$$I^{\rm cum}(\mathbf{s}) = \int |\mathbf{F}(\mathbf{s}; t)|^2 p(t)\,{\rm d}t, \tag{3}$$

where $p(t)$ is the pulse profile and $\mathbf{F}(\mathbf{s}; t)$ is a time-dependent structure factor,

$$\mathbf{F}(\mathbf{s}; t) = \sum_{j=1}^{N_{\rm atoms}} f_j(s; t)\exp(-B_j s^2/4)\exp[-2\pi i(\mathbf{s},\mathbf{r}_j)]. \tag{4}$$

Hereafter, time-independent atomic scattering factors are referred to as conventional atomic scattering factors and time-independent model structure factors are called conventional model structure factors, in contrast to the time-dependent values.

One of the purposes of our study was to examine to what extent the dependence of scattering factors on time affects the diffraction intensities. To answer this question, numerical tests were performed using the model of a cysteine-free and methionine-free mutant of dihydrofolate reductase (PDB entry 2d0k; Iwakura *et al.*, 2006). The number of scattered photons that hit a detector pixel is proportional to the incident beam fluence. The tests were performed at different values of the incident pulse fluence, which is the number of photons that cross a unit square in a pulse.

The first value, which is referred to below as low fluence, was 10^4 photons Å^{-2} per pulse. This value corresponds to the upper limit currently achievable for macromolecular crystals. The second value was 10^6 photons Å^{-2} per pulse. It is referred to below as moderate fluence and corresponds to an XFEL fluence that will be achievable in the near future. The third value, 10^8 photons Å^{-2} per pulse, is not yet attainable, but the rapid progress in the development of XFEL techniques allows us to consider it as non-fantastic. Below, we call this value high fluence. The results of our tests (§3) show that the changes caused by the time-dependence of the scattering factors are negligible at low fluence but become significant at moderate and high fluence values. Thus, with the implementation of the next generation of XFELs, scattering-factor evolution should be taken into account in precise calculations of diffraction intensities.

The basic problem that we address in this paper is the construction of an efficient practical scheme for the calculation of accumulated intensities (3). In structure solution by X-ray diffraction methods, the calculation of a set of theoretical values of intensities corresponding to a particular atomic model is a routine procedure, which is repeated hundreds of times for different trial values of atomic parameters. The computational efficiency of this step can play a key role in the practical feasibility of calculations and has been the subject of numerous studies (see Afonine & Urzhumtsev, 2004 and references therein). The idea of calculating instantaneous structure factors $\mathbf{F}(\mathbf{s}; t_k)$ for a series of time counts $t_1, \ldots, t_M$ and to use a numerical integration algorithm for immediate calculation of (3) is not attractive as it requires M times more

operations compared with the stationary case (equations 1 and 2). An alternative method is to transfer the integration in (3) to the only source of time-dependence, namely the scattering factors. This leads to the formula

$$I^{\rm cum}(\mathbf{s}) = \sum_{j,k=1}^{N_{\rm atoms}} A_{jk}(s) \exp[-(B_j + B_k)s^2/4] \exp[2\pi i(\mathbf{s}, \mathbf{r}_j - \mathbf{r}_k)], \tag{5}$$

where

$$A_{jk}(s) = \int f_j(s; t) f_k(s; t) p(t)\, {\rm d}t. \tag{6}$$

Integration (6) should be performed only once for particular XFEL experimental conditions (setup), while calculations of intensities using the formula (5) are repeated for every current set of atomic model parameters. The double sum in (5) makes direct calculations $N_{\rm atoms}$ times more time-consuming than calculations in the stationary case (equations 1 and 2). In this paper, we suggest an algorithm that allows the calculation of intensities (5) for a time exceeding the time of calculations in the case of stationary scattering not more than $n_{\rm types}$ times, where $n_{\rm types}$ is the relatively small number of chemically different elements in the structure being studied. Furthermore, within the resolution and accuracy limits typical for biological crystallography, the calculations can be performed for the same time as in the stationary case (equations 1 and 2).

It should be noted that the emission of electrons by atoms under the influence of an X-ray pulse is a stochastic process. This means that it is impossible to predict the order in which certain atoms lose electrons for a particular pulse. Here, we consider 'expected' time-dependent atomic electron-density distributions and scattering factors. In practice, this corresponds to averaging over a number of snapshots for similarly orientated objects, which gives a single X-ray image (White *et al.*, 2012, 2013). The fluctuations in individual time-dependent scattering factors give rise to an additional background in the image (Lorenz *et al.*, 2012). This background does not depend on individual atomic coordinates, and we do not touch upon the problem of background estimation in this paper.

2. Methods

2.1. Efficient calculation of cumulative intensities

Cumulative intensities (3) can be efficiently calculated as described below. The proof is presented in Appendix *A*. The approach suggested was essentially inspired by the paper of Lorenz *et al.* (2012), while some of its steps may also be found in other papers (Quiney & Nugent, 2011; Curwood *et al.*, 2013). The procedure consists of two parts. The first part should be performed only once for particular X-ray pulse parameters, whereas the second part is run many times for every new current set $\{\mathbf{r}_j, B_j\}$, $j = 1, \ldots, N_{\rm atoms}$ of model parameters. The efficiency of the algorithm is based on the hypothesis that the atomic model is composed of a large number of atoms, $N_{\rm atoms}$, whereas the number of different types of chemical elements in the model, $n_{\rm types}$, is relatively small, and that atoms of the same type have similar time-dependent scattering factors.

2.1.1. Auxiliary scattering factors. The first part of the calculations consists of three steps and, for every chemical type of atoms μ, results in a set of auxiliary scattering factors, $\tilde{f}_\mu^{(1)}(s), \ldots, \tilde{f}_\mu^{(n_{\rm types})}(s)$, calculated as functions of the scattering angle. We call the first of them the effective scattering factor $\tilde{f}_\mu^{(\rm eff)}(s)$ and the others the correcting scattering factors. We use the tilde symbol in $\tilde{f}_\mu(s)$ to indicate the scattering factors corresponding to the μth chemical element, while $f_j(s)$ stands for the jth atom in the model.

Step 1. For every chemical type μ, the time-dependent atomic scattering factor $\tilde{f}_\mu(s; t)$ is somehow estimated as a function of the scattering angle and time. We chose an approach based on the solution of a system of rate equations (see §2.2), although other approaches can also be tried.

Step 2. The time-averaged values of pairwise products of time-dependent form factors are calculated for every s value to form the moment matrix $\tilde{\mathbf{A}}(s)$,

$$\tilde{A}_{\mu\nu}(s) = \int \tilde{f}_\mu(s; t) \tilde{f}_\nu(s; t) p(t)\, {\rm d}t, \quad \mu, \nu = 1, \ldots, n_{\rm types}. \tag{7}$$

Step 3. An eigendecomposition of matrix $\tilde{\mathbf{A}}(s)$ is performed for every s value,

$$\tilde{\mathbf{A}} = \tilde{\mathbf{V}} \tilde{\mathbf{\Delta}} \tilde{\mathbf{V}}^T, \tag{8}$$

where $\tilde{\mathbf{\Delta}}$ is a diagonal matrix with the diagonal formed by the eigenvalues $\tilde{\delta}^{(1)}, \tilde{\delta}^{(2)}, \ldots, \tilde{\delta}^{(n_{\rm types})}$ of matrix $\tilde{\mathbf{A}}$, and the columns $\tilde{\mathbf{v}}^{(1)}, \tilde{\mathbf{v}}^{(2)}, \ldots, \tilde{\mathbf{v}}^{(n_{\rm types})}$ of matrix $\tilde{\mathbf{V}}$ form an orthonormal set of eigenvectors. It is supposed that the eigenvalues are enumerated in decreasing order. The values of the effective and correcting scattering factors are defined for the μth chemical type as

$$\begin{aligned} \tilde{f}_\mu^{\rm eff} &= \tilde{f}_\mu^{(1)} = [\tilde{\delta}^{(1)}]^{1/2} \tilde{v}_\mu^{(1)}, \\ \tilde{f}_\mu^{(2)} &= [\tilde{\delta}^{(2)}]^{1/2} \tilde{v}_\mu^{(2)}, \\ &\ldots, \\ \tilde{f}_\mu^{(n_{\rm types})} &= [\tilde{\delta}^{(n_{\rm types})}]^{1/2} \tilde{v}_\mu^{(n_{\rm types})}. \end{aligned} \tag{9}$$

The decomposition (8) is performed independently for every s value, making the eigenvalues and auxiliary scattering factors functions of s. Some consistency rules are applied to smooth the dependence of the found auxiliary scattering factors on s (see §2.1.4).

2.1.2. Superposition of diffraction patterns. The cumulative intensity for the current values of the atomic model parameters is calculated as a superposition of the effective intensity and its corrections,

$$I^{\rm cum}(\mathbf{s}) = \sum_{\alpha=1}^{n_{\rm types}} |\mathbf{F}^{(\alpha)}(\mathbf{s})|^2, \tag{10}$$

$$\mathbf{F}^{(\alpha)}(\mathbf{s}) = \sum_{j=1}^{N_{\rm atoms}} \tilde{f}_{\kappa(j)}^{(\alpha)}(s) \exp(-B_j s^2/4) \exp[2\pi i(\mathbf{s}, \mathbf{r}_j)], \quad \alpha = 1, \ldots, n_{\rm types}, \tag{11}$$

where $\kappa(j)$ is the chemical type of the jth atom in the list. The first term in the sum in (10),

$$I^{\rm eff}(\mathbf{s}) = |\mathbf{F}^{(1)}(\mathbf{s})|^2, \tag{12}$$

is referred to as the effective intensity. Auxiliary structure factors (11) are calculated as the usual structure factors with the exception that the sets of scattering factors are different. Any tricks to accelerate calculations (Afonine & Urzhumtsev, 2004) can be applied here. At the same time, in contrast to the conventional case, the intensity is not now just the squared structure-factor magnitude but is the sum of an effective value and a series of corrections. It is worth noting that corrections are applied to intensities, not directly to scattering factors or structure factors.

2.1.3. Approximation of the cumulative intensities. Equations (10) and (11) present the procedure for the exact calculation of cumulative intensities. Sometimes it can be simplified within the limits of acceptable accuracy. The significance of the correction $|\mathbf{F}^{(\alpha)}(\mathbf{s})|^2$ in (10) is determined by the ratio $\tilde{\delta}^{(\alpha)}(s)/\tilde{\delta}^{(1)}(s)$. The time of calculations may be reduced by using only the significant members in superposition (10),

$$I^{\rm cum}(\mathbf{s}) = \sum_{\alpha=1}^{\alpha_{\max}} |\mathbf{F}^{(\alpha)}(s)|^2. \tag{13}$$

In some cases (see §3.3), acceptable accuracy is reached by using only the principal member in the decomposition. The intensity is then calculated by means of conventional formulae with modified scattering factors,

$$I^{\rm cum}(\mathbf{s}) = |\mathbf{F}^{\rm eff}(\mathbf{s})|^2, \tag{14}$$

$$\mathbf{F}^{\rm eff}(\mathbf{s}) = \sum_{j=1}^{N} \tilde{f}^{\rm eff}_{\kappa(j)}(s) \exp(-B_j s^2/4) \exp[2\pi i(\mathbf{s}, \mathbf{r}_j)]. \tag{15}$$

These calculations have a computational cost similar to that in the conventional case.

We say that different time-dependent scattering factors $\tilde{f}_\mu(s; t)$, $\mu = 1, \ldots, n$ are synchronized if they are proportional to some common function of time

$$\tilde{f}_\mu(s; t) \simeq \gamma_\mu(s)\tilde{f}_0(s; t), \tag{16}$$

i.e. if their dependence on time is nearly the same for a particular s value. In this case, the moments in (7) may be presented as

$$\tilde{A}_{\mu\nu}(s) = \tilde{f}^{\rm sync}_\mu(s)\tilde{f}^{\rm sync}_\nu(s), \tag{17}$$

where

$$\tilde{f}^{\rm sync}_\mu(s) = \left\{\int [\tilde{f}_\mu(s; t)]^2 p(t)\, {\rm d}t\right\}^{1/2}, \tag{18}$$

which are the square roots of the diagonal elements of the matrix $\tilde{\mathbf{A}}$. The cumulative intensity in this case may be calculated similarly to as in equations (14) and (15), but with the use of $\tilde{f}^{\rm sync}_\mu(s)$ atomic scattering factors. It is worth noting that in this approach we do not need to know the coefficients $\gamma_\mu(s)$ and the 'consensus' scattering factor $\tilde{f}_0(s; t)$ in (16). It is enough to suppose that they exist. Such an approximation seems to be a little easier than that in (14) and (15) as it does not require calculation of the eigendecomposition (8) of the moment matrix. On the other hand, it is based on the synchronization hypothesis (16), which is not justified in advance, while the eigendecomposition does not produce too many difficulties for low-dimensional matrices.

The approach may further simplified by applying the concept of unitary factors as discussed by Lunin *et al.* (2013). In this case, a stricter form of synchronization is supposed,

$$\tilde{f}_\mu(s; t) \simeq Z_\mu \tilde{f}^{\rm unit}(s; t), \tag{19}$$

where Z_μ is the number of scattering electrons in the undamaged μth chemical type. This approach allows estimation of time-dependent scattering factors for different chemical elements supposing that the time-dependent scattering factor is known for only one element. A weak point of this approach is that the original hypothesis (19) seems to be poorly justified, especially for large fluence values, and can only be used for very rough estimates.

2.1.4. Consistency rules. The eigendecomposition (8) of the moment matrix is not unique even if the eigenvalues are properly numerated. The sign of any column in matrix $\tilde{\mathbf{V}}$ can be changed arbitrarily. The choice of a particular α and s of auxiliary scattering factors $\{-\tilde{f}^{(\alpha)}_\mu(s)\}$, $\mu = 1, \ldots, n_{\rm types}$ instead of $\{\tilde{f}^{(\alpha)}_\mu(s)\}$ does not influence the intensities as only the magnitudes of the structure factors (11) influence the result of the calculations. However, the continuity of $\tilde{f}^{(\alpha)}_\mu(s)$ (considered as a function of s) may be destroyed if the decompositions (8) performed for close s and $s + \Delta s$ values are not consistent in the signs of the eigenvectors. This is undesirable when the values of $\tilde{f}^{(\alpha)}_\mu(s)$ calculated at some grid values are then used for the interpolation of intermediate values. To avoid this problem, some consistency rules were applied when performing the eigendecomposition for a series of s values. Firstly, starting from the preliminary decomposition calculated at $s = 0$, the sign of every found vector $\tilde{\mathbf{v}}^{(\alpha)}(0)$ was changed if necessary to maximize the number of positive components, or, more precisely, to minimize the value

$$Q_{\rm pos} = \sum_{\kappa=1}^{n_{\rm types}} [\min\{0, \tilde{v}^{(\alpha)}_\kappa(0)\}]^2. \tag{20}$$

This value of $Q_{\rm pos}$ is equal to zero if all components of vector $\tilde{\mathbf{v}}^{(\alpha)}(0)$ are non-negative. Secondly, for two consecutive points s and $s + \Delta s$ the signs of the newly found vectors $\tilde{\mathbf{v}}^{(\alpha)}(s + \Delta s)$ were changed if necessary to have the minimal variance with the previously defined $\tilde{\mathbf{v}}^{(\alpha)}(s)$ vector,

$$Q_{\rm cons} = \sum_{\mu=1}^{n_{\rm types}} [\tilde{v}^{(\alpha)}_\mu(s) - \tilde{v}^{(\alpha)}_\mu(s + \Delta s)]^2 \Rightarrow \min. \tag{21}$$

The formulated consistency rule assumes implicitly that all eigenvalues of the moment matrix (7) are different and can be enumerated in descending order in a unique way. Theoretically, several eigenvalues may occasionally become equal. In this case, the maximization (21) should include additional degrees of freedom corresponding to the non-uniqueness of the choice of an orthonormal basis in the corresponding

eigensubspace. Here, we do not discuss this procedure in detail because on the one hand this event is rather theoretical in numerical calculations and on the other hand it only becomes important if scattering factors are interpolated for intermediate s values. Usually, the scattering factors of the electronic configurations and hence the time-dependent scattering factors can readily be calculated on a grid that is fine enough to avoid interpolation.

2.2. Simulation of time-dependent atomic scattering factors

We assume that each atom changes its state independently of other atoms. The time-dependent form factor of a scattering centre (an atom or an ion) is then determined by the time-dependent distribution of electrons over various atomic (ionic) shells, *i.e.* by populations of electronic configurations. These populations are found by solving a system of rate equations,

$$\frac{\mathrm{d}P_m(t)}{\mathrm{d}t} = \sum_{m' \neq m} [\Gamma_{mm'} P_{m'}(t) - \Gamma_{m'm} P_m(t)], \tag{22}$$

where $P_m(t)$ is the population of configuration m and $\Gamma_{mm'}$ is the rate of transition from configuration m to configuration m'. Photoionization in an inner shell followed by Auger decay is the dominant process at the photon energies currently used in X-ray diffraction studies. In addition, we considered the possibility of radiative decay (fluorescence). The latter is usually several orders of magnitude less probable than Auger decay for the same configuration, but fluorescence may be the only allowed channel for some configurations. Moreover, the transition rates of photoionization are proportional to the intensity of the incident radiation and alter during the pulse, while the rates of Auger decay and fluorescence are constant. It has been shown that these processes are indeed crucial for changes in the charge state of the molecule (Santra, 2009; Son *et al.*, 2011; Moribayashi, 2008). Next in importance are processes induced by secondary electrons and Compton scattering. The method of solving the rate equations for the populations has been used in studies of the effect of the degradation of a molecule on the resolving power of X-ray diffraction methods (Lorenz *et al.*, 2012; Lunin *et al.*, 2013; Sinitsyn *et al.*, 2013).

We calculated the subshell photoionization cross-sections with the wavefunctions obtained in the Hartree–Fock–Slater approximation (Herman & Skillman, 1963). The rates of the Auger and radiative transitions were taken from Moribayashi (2008), where they were obtained using the Cowan code (Cowan, 1968). The calculated photoionization cross-sections for C atoms and ions are in good agreement with calculations (Son *et al.*, 2011). The photoionization cross-section for hydrogen is negligible compared with the photoionization cross-sections for C, N and O.

Initially, all atoms of the molecule are in the ground-state configuration $1s^2 2s^2 2p^k$ (where $k = 2$ for C, $k = 3$ for N and $k = 4$ for O). In most cases, first the 1s inner shell is ionized. The photoionization cross-section at such a high photon energy is extremely small ($\sim 10^{-5}$ au at a photon energy of 8 keV). Nevertheless, if the photon flux density is of the order of 10^8 photons Å^{-2}, the inner shell photoionization rate is high despite the small cross-section. After photoionization in the 1s shell, other reaction channels are opened, Auger decay and fluorescence, followed in turn by an increase in the photoionization probability (*e.g.* for a given photon energy the photoionization cross-section of the 2p shell of the carbon ion C^+ is about two times higher than of the neutral atom). The charge density of the electronic shell gradually decreases during the atom evolution in the electromagnetic field. It is worth noting that even under the influence of such an intense photon flux, the atom does not have enough time to turn into bare nucleus (fully ionized). Our calculations show that for a radiation pulse with a FWHM of 10 fs and a peak intensity of 10^8 photons Å^{-2} at least one electron is left at the end of the pulse in 30% of C and O atoms and in 50% of N atoms. Most often the 2p electron and sometimes the 2s electron remain in the ion. The radiative transition to the ground state is the only allowed decay channel of the 2p state. Its probability is small, as well as the X-ray photoionization cross-section. This explains why the form factors of all of the atoms at high photon flux are similar (Figs. 1 and 3): in fact, all the ions are mostly in the same 2p state.

2.3. Comparison of conventional and time-dependent factors

2.3.1. Atomic scattering factors. It should be noted that the calculation of auxiliary scattering factors is not the final goal, but a tool for the calculation of theoretical intensity values. A common crystallographic practice in comparison of calculated and observed data is preliminary scaling of calculated (or observed) values to obtain the best correspondence between the two sets of values. Usually two global scaling coefficients are applied, namely the overall scaling factor $k_{\rm opt}$ and the overall atomic displacement parameter $B_{\rm opt}$. We apply a similar scaling to the two sets of scattering factors before their comparison. The reason is that the differences in scattering factors that can be removed by this scaling will be removed automatically at the structure-refinement step and so do not require immediate changes in the calculation procedures. The scaling coefficients $k_{\rm opt}$, $B_{\rm opt}$ applied in the comparison of two sets a and b of scattering factors for N, C and O atoms were determined by minimization of the weighted discrepancy,

$$R_f^{\rm cum} = \frac{N_{\rm C}\sum_s |f_{\rm C}^a(s) - \alpha(s) f_{\rm C}^b(s)| + N_{\rm N}\sum_s |f_{\rm N}^a(s) - \alpha(s) f_{\rm N}^b(s)| + N_{\rm O}\sum_s |f_{\rm O}^a(s) - \alpha(s) f_{\rm O}^b(s)|}{N_{\rm C}\sum_s |f_{\rm C}^a(s)| + N_{\rm N}\sum_s |f_{\rm N}^a(s)| + N_{\rm O}\sum_s |f_{\rm O}^a(s)|}, \tag{23}$$

where the summation extends over some grid of the resolution range $0 \leq s \leq s_{\max}$ and

$$\alpha(s) = k_{\rm opt} \exp(-B_{\rm opt} s^2/4). \tag{24}$$

The weights $N_{\rm C}$, $N_{\rm N}$ and $N_{\rm O}$ are equal to the number of atoms of the corresponding types in the test structure 2d0k.

2.3.2. Structure factors for a test structure. It is common practice in macromolecular crystallography to compare two diffraction patterns by calculation of the discrepancy index

between the two sets of structure-factor magnitudes, while sometimes the measure of quality is based on discrepancies in the intensities. In the nonstationary case the intensities are accumulated with time, so the intensities $I^{\rm cum}(s)$ seem to be natural values for comparison with others. Nevertheless, to transform the calculated discrepancies onto a more familiar scale, we introduce artificial magnitudes

$$F^{\rm cum}(\mathbf{s}) = [I^{\rm cum}(\mathbf{s})]^{1/2} \qquad (25)$$

and use them to calculate standard R factors. In our test, we used two types of R factors, namely 'shell' R factors $R^{\rm shell}(s^*)$ calculated for a thin spherical shell $s^* \leq s \leq s^* + \Delta s$ and 'cumulative' R factors $R^{\rm cum}(s^*)$ calculated for extended spherical volumes $0 \leq s \leq s^*$. During the calculation of shell factors, the scaling coefficients $k_{\rm opt}$, $B_{\rm opt}$ were fixed for all shells at some previously determined values, while the optimization for cumulative R factors was performed individually for every sphere $0 \leq s \leq s^*$.

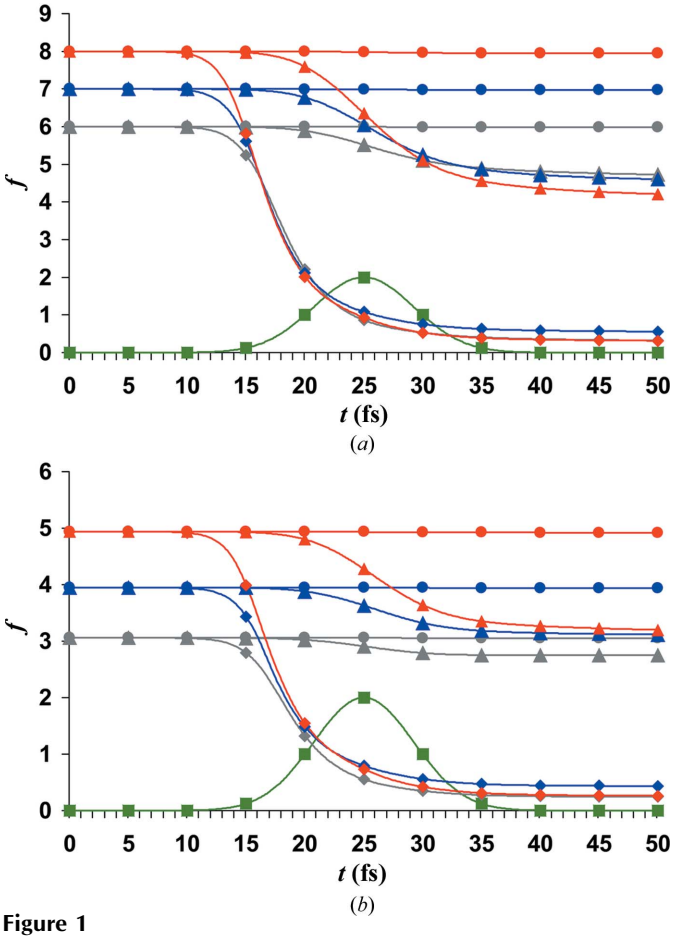

Figure 1
Time-dependence of atomic scattering factors for scattering angles corresponding to $\sin\theta/\lambda = 0$ (*a*) and $\sin\theta/\lambda = 0.25$ (*b*). The scattering factors for C, N and O atoms are shown in grey, blue and red, respectively. Circles, triangles and squares denote graphs for fluence values of 10^4, 10^6 and 10^8 photons Å^{-2} per pulse, respectively. The profile of the pulse (in relative values) is shown in green.

2.4. Test object

The atomic model of a cysteine-free and methionine-free mutant of *Escherichia coli* dihydrofolate reductase (Iwakura *et al.*, 2006; PDB entry 2d0k) was used in our tests. This protein crystallized in space group *C*2 with unit-cell parameters $a = 79.58$, $b = 56.69$, $c = 85.14$ Å, $\beta = 106.81^\circ$. Two molecules of 159 residues each are present in the asymmetric part of the unit cell. The molecules do not contain S atoms; the number of C, N, and O atoms is 1660, 450 and 702, respectively. Cl atoms (one per molecule) were excluded from the calculations. For the analysis, we chose a protein without S atoms in order to avoid laborious calculations of numerous unknown cross-sections and rates of transition between atomic configurations.

3. Results

3.1. Time-dependent scattering factors

The time-dependent scattering factors for C, N and O atoms were calculated as described in §2.2 for three levels of fluence: 10^4, 10^6 and 10^8 photons Å^{-2} per pulse. The energy of the photons was supposed to be 8 keV ($\lambda = 1.55$ Å). The profile of the pulse $p(t)$ was supposed to be Gaussian with FWHM = 10 fs. Fig. 1 shows the time variation of time-dependent scattering factors for two scattering angles and different fluence levels. Similar to other results discussed below, a fluence of 10^4 photons Å^{-2} per pulse does not lead to significant changes in the diffraction pattern. The larger values of fluence result in changes that should be taken into account in accurate studies.

The calculated time-dependent scattering factors were used for calculation of the moment matrix $\tilde{\mathbf{A}}(s)$ (7), its eigenvalues and eigenvectors. The eigendecomposition (8) was performed for every s value independently, and the consistency rules were applied to resolve the ambiguity as described in §2.1.4. Fig. 2 shows the eigenvalues as functions of scattering angle for different fluence levels. For low fluence, the second and third egenvalues are approximately 10^6 times less than the principal value $\tilde{\delta}^{(1)}$ and the corresponding corrections in (10) are negligible. For moderate fluence, the third eigenvalue is negligible, while the second eigenvalue may be essential in accurate calculations. For high fluence, both $\tilde{\delta}^{(2)}$ and $\tilde{\delta}^{(3)}$ should be kept in mind. Below, we discuss the influence of correcting terms.

The analysis of eigenvalues in the previous section showed that the diffraction pattern is mostly defined by effective scattering factors. Fig. 3 shows effective scattering factors and conventional scattering factors for two fluence levels. For low fluence (10^4 photons Å^{-2} per pulse) the difference is invisible, and the corresponding plot is omitted. Fig. 4 shows correcting scattering factors $\tilde{f}_\mu^{(2)}(s)$ for a fluence of 10^6 photons Å^{-2} per pulse and $\tilde{f}_\mu^{(2)}(s)$ and $\tilde{f}_\mu^{(3)}(s)$ for a fluence of 10^8 photons Å^{-2} per pulse. As seen from the analysis of the eigenvalues, these corrections are negligible at low and medium resolutions but may be essential when the resolution approaches 1 Å ($\sin\theta/\lambda = 0.5$) or better.

In calculations of intensities, effective scattering factors may be considered to some extent as an analogue of usual scat-

tering factors adapted to the conditions of a particular XFEL experiment. To compare them with conventional scattering factors, the discrepancy index was calculated for thin resolution shells as

$$R_f^{\rm shell}(s) = R_f^{\rm shell}(s; k_{\rm opt}, B_{\rm opt}) = \frac{N_{\rm C}|f_{\rm C}^{\rm st}(s) - \alpha(s) f_{\rm C}^{\rm eff}(s)| + N_{\rm N}|f_{\rm N}^{\rm st}(s) - \alpha(s) f_{\rm N}^{\rm eff}(s)| + N_{\rm O}|f_{\rm O}^{\rm st}(s) - \alpha(s) f_{\rm O}^{\rm eff}(s)|}{N_{\rm C}\sum_s |f_{\rm C}^{\rm st}(s)| + N_{\rm N}\sum_s |f_{\rm N}^{\rm st}(s)| + N_{\rm O}\sum_s |f_{\rm O}^{\rm st}(s)|}, \quad (26)$$

where $f^{\rm st}$ and $f^{\rm eff}$ represent conventional and effective scattering factors and $\alpha(s) = k_{\rm opt}\exp(-B_{\rm opt}s^2/4)$. The overall scaling coefficients $k_{\rm opt}$, $B_{\rm opt}$ are applied to minimize the discrepancy for the whole resolution range (∞–1 Å; see §2.3.1). The weights $N_{\rm C}$, $N_{\rm N}$ and $N_{\rm O}$ are equal to the numbers of corresponding atoms in the test structure 2d0k. The optimal values of the scaling coefficients are summarized in Table 1. Fig. 5 shows that this discrepancy is negligible for a fluence of 10^4 photons Å^{-2} per pulse but approaches 5% for a fluence of 10^6 photons Å^{-2} per pulse and 10% for a fluence of 10^8 photons Å^{-2} per pulse. Fig. 6 shows the optimally scaled effective scattering factors in comparison with conventional scattering factors for the medium fluence of 10^6 photons Å^{-2} per pulse.

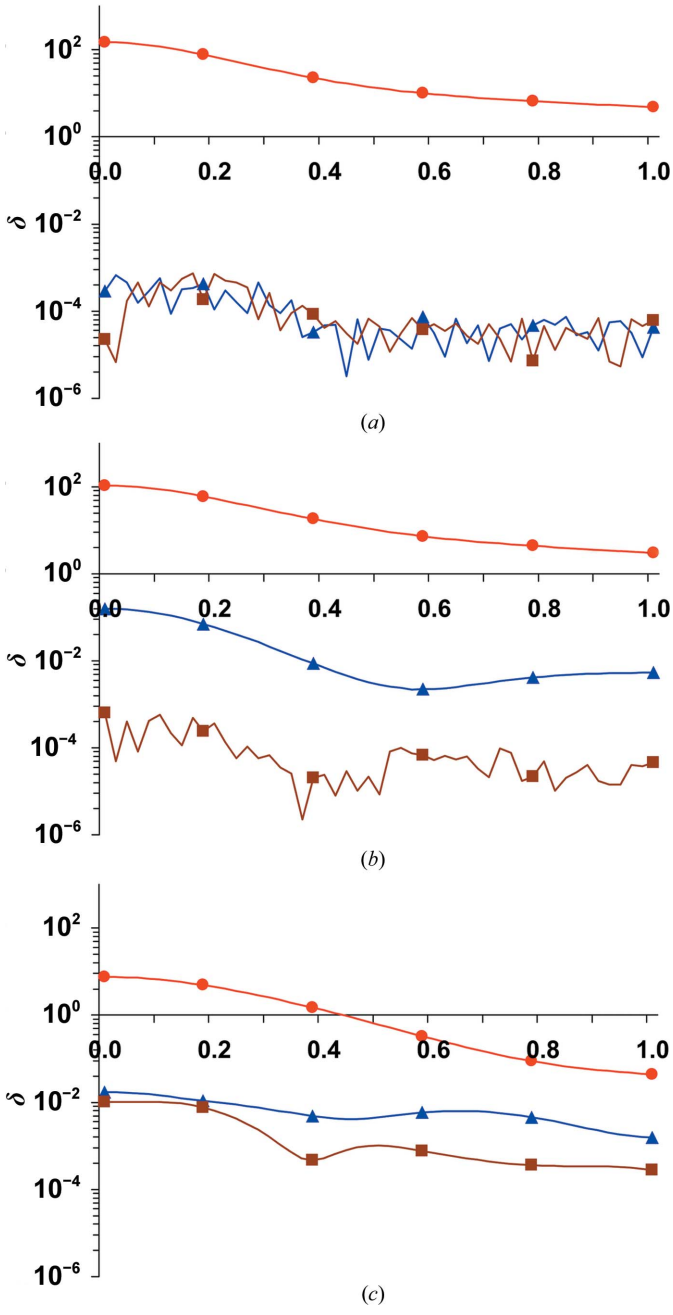

Figure 2
Eigenvalues $\tilde{\delta}^{(1)} > \tilde{\delta}^{(2)} > \tilde{\delta}^{(3)}$ of the moment matrix (7) as functions of $\sin\theta/\lambda$ are shown in red (circles), blue (triangles) and brown (squares), respectively. The fluence levels are 10^4 photons Å^{-2} per pulse (*a*), 10^6 photons Å^{-2} per pulse (*b*) and 10^8 photons Å^{-2} per pulse (*c*).

3.2. Cumulative intensities and structure factors in the case of nonstationary scattering

Three-dimensional sets of structure factors calculated for PDB entry 2d0k in stationary and nonstationary cases were compared by calculating the standard *R* factors for thin resolution shells and extending zones (0, $s_{\rm max}$) (Fig. 7). The developed fast algorithm for calculation of cumulative intensities (§2.1) was used in the nonstationary case. For the low

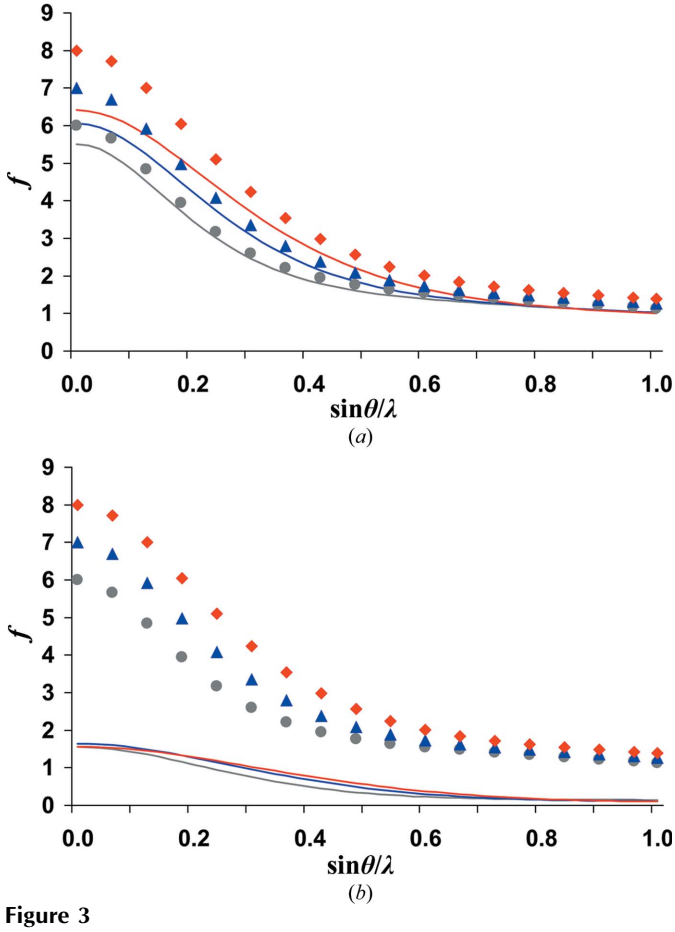

Figure 3
Conventional scattering factors (markers) and effective values of time-dependent scattering factors (lines) are shown for C, N and O atoms (grey, blue and red, respectively). Two fluence levels, 10^6 photons Å^{-2} per pulse (*a*) and 10^8 photons Å^{-2} per pulse (*b*), are shown.

Table 1
Optimal scaling coefficients for the sets of conventional and effective scattering factors for C, N and O atoms.

Fluence (photons Å^{-2} per pulse)	k_{opt}	B_{opt}	R_f^{cum}
10^4	1.001	0.0	0.000
10^6	1.089	0.0	0.040
10^8	3.779	0.5	0.099

fluence value, only effective scattering factors were taken into account, since corrections in this case are negligible. For the moderate fluence, two variants for calculation of cumulative intensities were tested, one with the main term $|\mathbf{F}^{eff}(\mathbf{s})|^2$ only in (10) and the other with the main term and the correction $|\mathbf{F}^{(2)}(\mathbf{s})|^2$. Similarly, for the high fluence the calculations were performed with the main term only and with the use of two corrections $|\mathbf{F}^{(2)}(\mathbf{s})|^2$ and $|\mathbf{F}^{(3)}(\mathbf{s})|^2$. In calculations of shell R factors, the scaling factors were the same for all resolution shells and were determined by optimizing the overall R factor in the 1 Å resolution zone. In calculations of the 'cumulative' factors R^{cum}, the scaling factors were determined separately for every zone $0 \leq s \leq s_{max} = 1/d$.

It follows from these figures that the effect of nonstationarity is negligible at a fluence of 10^4 photons Å^{-2} per pulse.

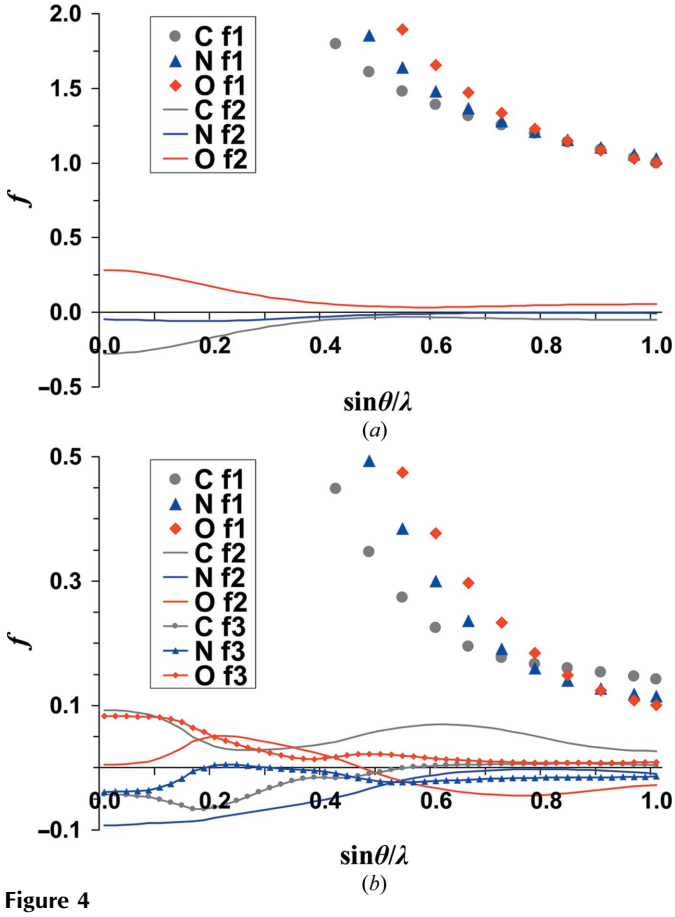

Figure 4
Effective (markers) and correcting (lines) scattering factors for fluence levels of 10^6 photons Å^{-2} per pulse (*a*) and 10^8 photons Å^{-2} per pulse (*b*). Scattering factors for C, N and O atoms are shown in grey, blue and red, respectively.

Nevertheless, even in this case correction for nonstationarity for high-resolution reflections might improve the accuracy in high-resolution shells. For larger fluence values, the effect of time-dependence of scattering factors is much more prominent and should be taken into account.

3.3. Accuracy of simplified approaches

Analysis of the eigenvalues of the moment matrix (7) and a comparison of the results of calculations performed with and without high-order corrections (Fig. 7) show that even for the case of large fluence values approximation of the calculated intensity by the principal value is accurate enough. To estimate the intensity more precisely, crystallographic R factors were calculated between sets of structure-factor magnitudes calculated with and without additional corrections. The maximal difference R^{shell} in resolution shells (up to 1 Å resolution) did not exceed 0.002 for a fluence of 10^6 photons Å^{-2} per pulse and 0.014 for a fluence of 10^8 photons Å^{-2} per pulse (below 0.005 in the resolution zone to 1.2 Å). This means that with

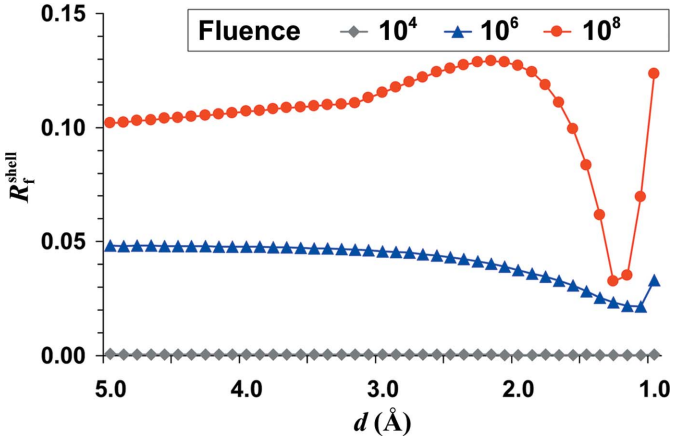

Figure 5
Comparison of conventional and effective scattering factors. Discrepancy index (26) as a function of resolution for a set of optimally scaled C, N and O scattering curves.

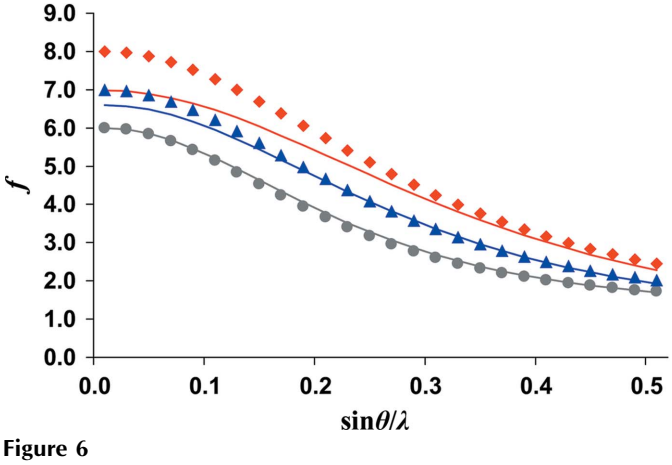

Figure 6
Optimally scaled effective scattering factors (lines) in comparison with conventional scattering factors (markers) for a fluence level of 10^6 photons Å^{-2} per pulse. Scattering factors for C, N and O atoms are shown in grey, blue and red, respectively.

these fluence values and resolution ranges, the approximation of calculated intensities by the principal value

$$I^{\rm cum}(\mathbf{s}) \simeq |\sum_{j=1}^{N_{\rm atoms}} f_j^{\rm eff}(s)\exp(-B_j s^2/4)\exp[-2\pi i(\mathbf{s},\mathbf{r}_j)]|^2 \quad (27)$$

is accurate enough for practical work with biological macromolecules. At the same time, the use of effective scattering factors instead of conventional scattering factors is essential for accuracy in work with medium and high fluence values.

As mentioned in §2.1.3, in the approximation of synchronized scattering factors the intensities can be calculated using auxiliary factors calculated as the square roots of the time-averaged squares of the time-dependent scattering factors (18). In our tests, comparison of these scattering factors with the effective scattering factors did not reveal a significant difference. Even for the largest tested fluence, the values of shell discrepancy factors (26) did not exceed 0.005 for the high-resolution shells. Thus, for the fluence values considered the differences in the time-dependence of scattering factors of different atom types are negligible, and effective scattering factors may be estimated by the square roots of the time-averaged squares of the time-dependent scattering factors

$$\tilde{f}_\mu^{\rm eff}(s) \simeq \tilde{f}_\mu^{\rm synch}(s) = \left[\int \tilde{f}_\mu(s;t)^2 p(t)\,{\rm d}t\right]^{1/2}. \quad (28)$$

(28) and (27) present the most straightforward method for the calculation of cumulative diffraction intensities corrected for the time-dependence of atomic electron configurations.

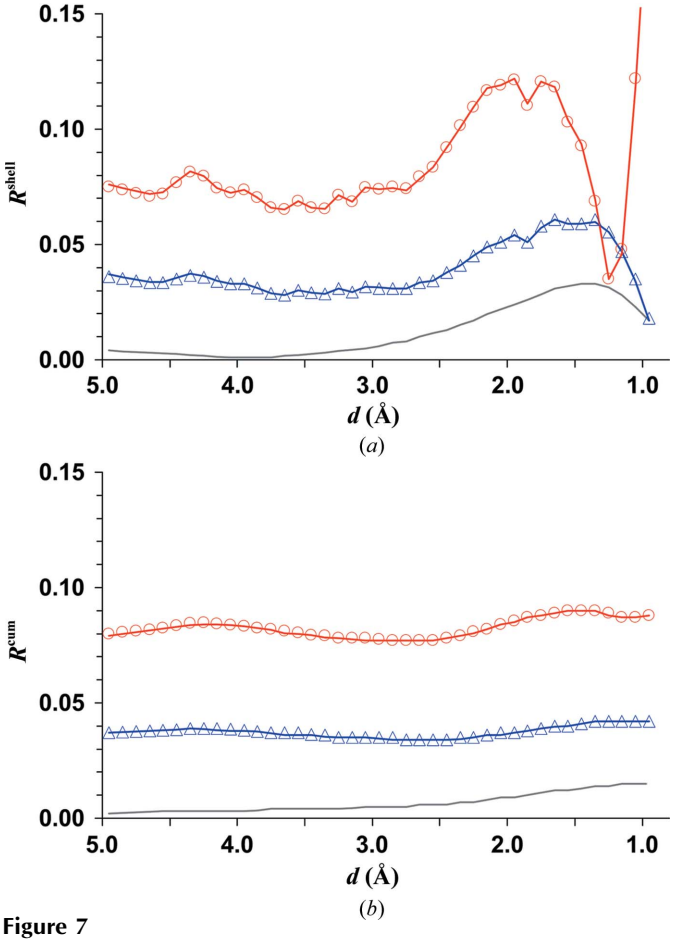

Figure 7
Comparison of calculated conventional structure factors for PDB entry 2d0k with the structure factors corresponding to modelled nonstationary cases. Crystallographic *R* factors are shown for thin resolution shells (*a*) and for extending resolution zones (*b*). Three modelled fluence levels of 10^4, 10^6 and 10^8 photons Å^{-2} per pulse are shown in grey, blue and red, respectively. Solid lines show the results obtained with the use of the main term in (10) only. Open circles and triangles show *R* factors accounting for correcting terms.

4. Conclusions

In the case of nonstationary scattering, straightforward calculation of the diffraction pattern is significantly more time-consuming than in the conventional case. The use of eigen-decomposition of the time-averaged matrix of the pairwise products of time-dependent scattering factors allows one to present the diffraction pattern as a superposition of an 'effective' and a finite series of 'correcting' patterns. The number of terms in the superposition does not exceed the number of chemically different types of atoms in the studied object and is small for biological macromolecules. The effective and correcting diffraction patterns may be calculated in the usual way for biological crystallography and each requires the same time for calculation as a conventional pattern. The only difference is the use in the calculations of specially derived effective and correcting atomic scattering factors instead of the tabulated values. The derived scattering factors depend on XFEL experiment parameters and are calculated individually for a particular XFEL experiment.

Simulation of nonstationary diffraction by solving the rate equations for the populations of electronic configurations demonstrated that the influence of nonstationarity is negligible for a photon fluence of up to 10^4 photons Å^{-2} per pulse, which is the upper limit achieved in experiments with biological macromolecular crystals. At the same time, for higher fluence values, which are expected in the near future, nonstationarity becomes as essential factor. The corresponding corrections of calculated intensity values should be taken into account in calculations.

Simulation of diffraction patterns for a test protein demonstrated that for the considered fluence range (10^4, 10^6 and 10^8 photons Å^{-2} per pulse) the correcting terms are negligible within the reasonable accuracy for biological crystallography. As a result, the diffraction pattern may be approximated by the principal term of the decomposition, *i.e.* by the sole effective term. Generally, the corresponding atomic scattering factors are the components of the principal eigenvector in the eigendecomposition, which, however, can be approximated in a simpler way as the square roots of time-averaged squares of time-dependent scattering factors.

APPENDIX *A*
An efficient calculation of cumulative intensities

The approach suggested was essentially inspired by the paper of Lorenz *et al.* (2012). In the stationary case, the computa-

tional complexity of a straightforward calculation of the intensity $I(\mathbf{s})$ for a particular $\mathbf{s}$ value using the formula

$$I(\mathbf{s}) = \sum_{j,k=1}^{N_{\rm atoms}} f_j(s) f_k(s) \exp[-(B_j + B_k)s^2/4] \exp[2\pi i(\mathbf{s}, \mathbf{r}_j - \mathbf{r}_k)] \quad (29)$$

is proportional to $(N_{\rm atoms})^2$, but it becomes proportional to the first power $N_{\rm atoms}$ if organized as a two-step procedure (equations 1 and 2). This trick is unusable in the nonstationary case (equations 5 and 6) since generally the elements of the moment matrix $\mathbf{A} = ((A_{jk}))$ defined by (6) cannot be presented in the form $A_{jk} = a_j a_k$. Nevertheless, one can present the matrix $\mathbf{A}$ as a sum of simpler matrices

$$\mathbf{A} = \sum_{\alpha=1}^{N_{\rm atoms}} \delta^{(\alpha)} \mathbf{A}^{(\alpha)}, \quad (30)$$

where each of the matrices $\mathbf{A}^{(\alpha)}$, $\alpha = 1, 2, \ldots, N_{\rm atoms}$ has a desired form

$$A_{jk}^{(\alpha)} = a_j^{(\alpha)} a_k^{(\alpha)}. \quad (31)$$

This follows from the eigendecomposition of the real symmetric matrix

$$\mathbf{A} = \mathbf{V}\mathbf{\Delta}\mathbf{V}^T. \quad (32)$$

Here, $\mathbf{\Delta}$ is the diagonal matrix whose elements are the corresponding eigenvalues of the matrix $\mathbf{A}$, and the columns of the matrix $\mathbf{V}$ are an orthonormal set of eigenvectors. Let $a_1^{(\alpha)}, a_2^{(\alpha)}, \ldots, a_{N_{\rm atoms}}^{(\alpha)}$ denote the components of the αth eigenvector (*i.e.* the αth column of matrix $\mathbf{V}$). Decomposition (30) then takes the form

$$A_{jk} = \sum_{\alpha=1}^{N_{\rm atoms}} \delta^{(\alpha)} a_j^{(\alpha)} a_k^{(\alpha)}. \quad (33)$$

The intensity (5) may now be presented as

$$I^{\rm cum}(\mathbf{s}) = \sum_{\alpha=1}^{N_{\rm atoms}} \delta^{(\alpha)} |\hat{\mathbf{F}}^{(\alpha)}(\mathbf{s})|^2, \quad (34)$$

where the auxiliary cumulative structure factors $\hat{\mathbf{F}}^{(\alpha)}(s)$ are calculated by the usual formula for structure factors, but with artifical scattering factors $a_j(\alpha)(s)$,

$$\hat{\mathbf{F}}^{(\alpha)}(\mathbf{s}) = \sum_{j=1}^{N_{\rm atoms}} a_j^{(\alpha)}(s) \exp(-B_j s^2/4) \exp[-2\pi i(\mathbf{s}, \mathbf{r}_j)]. \quad (35)$$

As has previously been noted in the literature (Quiney & Nugent, 2011; Lorenz *et al.*, 2012; Curwood *et al.*, 2013), (34) is equivalent to the modal decomposition of Wolf (1982) and is often referred to as a sum of coherent modes. In this paper, we consider this decomposition just as a formal mathematical presentation, without attempting to ascribe any physical meaning to it.

The calculation of intensities by means of (35) and (34) still requires $N_{\rm atoms}$ times more operations compared with the stationary case, but it can be drastically reduced if the number of chemically different elements is small enough. Biological macromolecules consist of a large number of atoms, but the number of different elements is mostly limited to H, C, N, O and S atoms. Let $n_{\rm types}$ be the number of different elements in the structure and $\kappa(j)$ be a function that assigns to the jth atom (in the full list of atoms) its type number κ. Let $\tilde{f}_\mu(s; t)$ be a form factor for the μth chemical element. (We use the tilde symbol to mark a scattering factor corresponding to a type of atom, not to a particular atom in the model.) Let

$$\mathbf{T}_\mu(\mathbf{s}) = \sum_{j:\kappa(j)=\mu} \exp(-B_j s^2/4) \exp[-2\pi i(\mathbf{s}, \mathbf{r}_j)], \quad \mu = 1, 2, \ldots, n_{\rm types} \quad (36)$$

be the partial sum for atoms of the μth type so that

$$\mathbf{F}(\mathbf{s}; t) = \sum_{\mu=1}^{n_{\rm types}} \tilde{f}_\mu(s; t) \mathbf{T}_\mu(\mathbf{s}). \quad (37)$$

Formula (5) for the cumulative intensity becomes

$$I^{\rm cum}(\mathbf{s}) = \sum_{\nu,\mu=1}^{n_{\rm types}} \tilde{A}_{\mu\nu} \mathbf{T}_\mu \overline{\mathbf{T}}_\nu, \quad (38)$$

where $\overline{\mathbf{T}}$ denotes the conjugate of the complex number $\mathbf{T}$ and

$$\tilde{A}_{\mu\nu}(s) = \int \tilde{f}_\mu(s; t) \tilde{f}_\nu(s; t) p(t)\, \mathrm{d}t. \quad (39)$$

Let matrix $\tilde{\mathbf{A}}$ be presented as

$$\tilde{\mathbf{A}} = \tilde{\mathbf{V}}\tilde{\mathbf{\Delta}}\tilde{\mathbf{V}}^T, \quad (40)$$

where $\mathbf{\Delta}$ is the diagonal matrix with the diagonal formed by the eigenvalues $\tilde{\delta}^{(1)}, \tilde{\delta}^{(2)}, \ldots, \tilde{\delta}^{(n_{\rm types})}$ of matrix $\tilde{\mathbf{A}}$ and columns $\tilde{\mathbf{v}}^{(1)}, \tilde{\mathbf{v}}^{(2)}, \ldots, \tilde{\mathbf{v}}^{(n_{\rm types})}$ of matrix $\mathbf{V}$ are an orthonormal set of eigenvectors. Formula (40) implies that

$$\tilde{A}_{\mu\nu} = \sum_{\alpha=1}^{n_{\rm types}} \tilde{\delta}^{(\alpha)} \tilde{v}_\mu^{(\alpha)} \tilde{v}_\nu^{(\alpha)} = \sum_{\alpha=1}^{n_{\rm types}} \tilde{f}_\mu^{(\alpha)} \tilde{f}_\nu^{(\alpha)}, \quad (41)$$

with

$$\tilde{f}_\mu^{(\alpha)} = [\tilde{\delta}^{(\alpha)}]^{1/2} \tilde{v}_\mu^{(\alpha)}, \quad (42)$$

supposing that the eigenvalues are non-negative. The cumulative intensity can be now calculated as

$$I^{\rm cum}(\mathbf{s}) = \sum_{\alpha=1}^{n_{\rm types}} \sum_{\nu,\mu=1}^{n_{\rm types}} \tilde{f}_\mu^{(\alpha)} \tilde{f}_\nu^{(\alpha)} \mathbf{T}_\mu \overline{\mathbf{T}}_\nu = \sum_{\alpha=1}^{n_{\rm types}} \left| \sum_{\mu=1}^{n_{\rm types}} \tilde{f}_\mu^{(\alpha)} \mathbf{T}_\mu \right|^2 = \sum_{\alpha=1}^{n_{\rm types}} |\mathbf{F}^{(\alpha)}(\mathbf{s})|^2, \quad (43)$$

where

$$\mathbf{F}^{(\alpha)}(\mathbf{s}) = \sum_{j=1}^{N} \tilde{f}_{\kappa(j)}^{(\alpha)}(s) \exp(-B_j s^2/4) \exp[-2\pi i(\mathbf{s}, \mathbf{r}_j)]. \quad (44)$$

As the result, the diffraction pattern in the nonstationary case may be calculated as the sum of a small number $n_{\rm types}$ of stationary patterns $I^{(\alpha)}(\mathbf{s}) = |\mathbf{F}^{(\alpha)}(\mathbf{s})|^2$, which can be calculated in a conventional way by the squared magnitude of quasi-stationary structure factors (44). These structure factors resemble the usual form of structure factors, with the only difference being in the scattering factors, which are now auxiliary values determined by decomposition (40). The computational complexity of these calculations exceeds that for the stationary case by a small factor $n_{\rm types}$ and can some-

times be reduced to the complexity of stationary diffraction calculations if some $I^{(\alpha)}(\mathbf{s})$ are negligible.

The decomposition (40) is not unique. For example, the eigenvalues may be renumbered, which results in permutation of the columns of matrix $\tilde{\mathbf{V}}$. We suppose that the eigenvalues are numbered in descending order, so that we can consider $I^{(1)}(\mathbf{s}) = |\mathbf{F}^{(1)}(\mathbf{s})|^2$ as the principal term in decomposition (21) and the next terms as corrections. We call the auxiliary scattering factors $\tilde{f}_\mu^{(1)}(s)$ the 'effective' value $\tilde{f}_\mu^{\rm eff}(s)$ of the time-dependent scattering factor and $\tilde{f}_\mu^{(2)}(s)$, ..., $\tilde{f}_\mu^{(n_{\rm types})}(s)$ the correcting scattering factors. It should be emphasized that the correcting scattering factors are not added to the effective scattering factors directly. They are used as auxiliary entities for the calculation of the correcting intensities summed in (43).

The work was partially supported by RFBR grants 13-04-00118 and 14-04-31608. The authors acknowledge the financial support of the Ministry of Education and Science of the Russian Federation (Contract 07.514.11.4126).

References

Afonine, P. V. & Urzhumtsev, A. (2004). *Acta Cryst.* A**60**, 19–32.

Barends, T. R. M., Foucar, L., Botha, S., Doak, R. B., Shoeman, R. L., Nass, K., Koglin, J. E., Williams, G. J., Boutet, S., Messerschmidt, M. & Schlichting, I. (2014). *Nature (London)*, **505**, 244–247.

Barends, T. R. M. *et al.* (2013). *Acta Cryst.* D**69**, 838–842.

Barty, A. *et al.* (2012). *Nature Photonics*, **6**, 35–40.

Bergh, M., Huldt, G., Tîmneanu, N., Maia, F. R. N. C. & Hajdu, J. (2008). *Q. Rev. Biophys.* **41**, 181–204.

Boutet, S. *et al.* (2012). *Science*, **337**, 362–364.

Chapman, H. N. *et al.* (2011). *Nature (London)*, **470**, 73–77.

Cowan, R. D. (1968). *J. Opt. Soc. Am.* **58**, 808–818.

Curwood, E. K., Quiney, H. M. & Nugent, K. A. (2013). *Phys. Rev. A*, **87**, 053407.

Hau-Riege, S. P., London, R. A. & Szoke, A. (2004). *Phys. Rev. E*, **69**, 051906.

Henderson, R. (1995). *Q. Rev. Biophys.* **28**, 171–193.

Herman, F. & Skillman, S. (1963). *Atomic Structure Calculations.* Englewood Cliffs: Prentice-Hall Inc.

Iwakura, M., Maki, K., Takahashi, H., Takenawa, T., Yokota, A., Katayanagi, K., Kamiyama, T. & Gekko, K. (2006). *J. Biol. Chem.* **281**, 13234–13246.

Johansson, L. C. *et al.* (2012). *Nature Methods*, **9**, 263–265.

Johansson, L. C. *et al.* (2013). *Nature Commun.* **4**, 2911.

Kern, J. *et al.* (2012). *Proc. Natl Acad. Sci. USA*, **109**, 9721–9726.

Kern, J. *et al.* (2013). *Science*, **340**, 491–495.

Krause, M. O. & Oliver, J. H. (1979). *J. Phys. Chem. Ref. Data*, **8**, 329–338.

Lomb, L. *et al.* (2011). *Phys. Rev. B*, **84**, 214111.

Lorenz, U., Kabachnik, N. M., Weckert, E. & Vartanyants, I. (2012). *Phys. Rev. E*, **86**, 051911.

Lunin, V. Y., Grum-Grzhimailo, A. N., Gryzlova, E. V., Sinitsyn, D. O., Balabaev, N. K., Lunina, N. L., Petrova, T. E., Tereshkina, K. B., Abdulnasyrov, E. G., Stepanov, A. S. & Krupyanskii, Y. F. (2013). *Math. Biol. Bioinform.* **8**, 93–118.

Moribayashi, K. (2008). *J. Phys. B At. Mol. Opt. Phys.* **41**, 085602.

Neutze, R., Wouts, R., van der Spoel, D., Weckert, E. & Hajdu, J. (2000). *Nature (London)*, **406**, 752–757.

Quiney, H. M. & Nugent, A. K. (2011). *Nature Phys.* **7**, 142–146.

Redecke, L. *et al.* (2013). *Science*, **339**, 227–230.

Santra, R. (2009). *J. Phys. B At. Mol. Opt. Phys.* **42**, 023001.

Sinitsyn, D. O., Lunin, V. Y., Grum-Grzhimailo, A. N., Gryzlova, E. V., Balabaev, N. K., Lunina, N. L., Petrova, T. E., Tereshkina, K. B., Abdulnasyrov, E. G., Stepanov, A. S. & Krupyanskii, Y. F. (2013). *Nanostruct. Math. Phys. Model.* **9**, 5–32.

Son, S. K., Young, L. & Santra, R. (2011). *Phys. Rev. A*, **83**, 033402.

White, T. A., Barty, A., Stellato, F., Holton, J. M., Kirian, R. A., Zatsepin, N. A. & Chapman, H. N. (2013). *Acta Cryst.* D**69**, 1231–1240.

White, T. A., Kirian, R. A., Martin, A. V., Aquila, A., Nass, K., Barty, A. & Chapman, H. N. (2012). *J. Appl. Cryst.* **45**, 335–341.

Wolf, E. (1982). *J. Opt. Soc. Am.* **72**, 343–351.